Northumbria University
NEWCASTLE

University**Library**

Journal Pre-proof

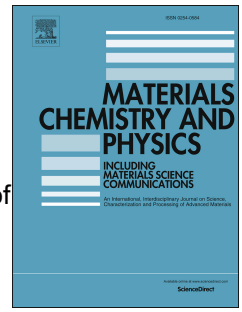

Highly stable, love-mode surface acoustic wave biosensor using Au nanoparticle-MoS_2-rGO nano-cluster doped polyimide nanocomposite for the selective detection of carcinoembryonic antigen

P.J. Jandas, Jingting Luo, K. Prabakaran, Fu Chen, Yong Qing Fu

PII: S0254-0584(20)30179-6

DOI: https://doi.org/10.1016/j.matchemphys.2020.122800

Reference: MAC 122800

To appear in: *Materials Chemistry and Physics*

Received Date: 25 October 2019

Revised Date: 4 February 2020

Accepted Date: 12 February 2020

Please cite this article as: P.J. Jandas, J. Luo, K. Prabakaran, F. Chen, Y.Q. Fu, Highly stable, love-mode surface acoustic wave biosensor using Au nanoparticle-MoS_2-rGO nano-cluster doped polyimide nanocomposite for the selective detection of carcinoembryonic antigen, *Materials Chemistry and Physics* (2020), doi: https://doi.org/10.1016/j.matchemphys.2020.122800.

Highly stable, love-mode surface acoustic wave biosensor using Au nanoparticle-MoS_2-rGO nano-cluster doped polyimide nanocomposite for the selective detection of carcinoembryonic antigen

P J Jandas[a], Jingting Luo[a,b]*, K. Prabakaran[a], Fu Chen[a]*, Yong Qing Fu[c]

[a]Key Laboratory of Optoelectronic Devices and Systems of Ministry of Education and Guangdong Province, College of Physics and Optoelectronic Engineering, Shenzhen University, 518060, Shenzhen, PR China

[b]State Key Laboratory of Powder Metallurgy, Central South University, Changsha, PR China

[c]Faculty of Engineering and Environment, Northumbria University, Newcastle upon Tyne, NE1 8ST, UK

*Prof. Jingting Luo

Shenzhen Key Laboratory of Advanced Thin Films and Applications,

College of Physics and Energy,

Shenzhen University,

Pin: 518060, Shenzhen, PR China

Email: luojt@szu.edu.in, chenfu@szu.edu.cn

Highly stable, love-mode surface acoustic wave biosensor using Au nanoparticle-MoS_2-rGO nano-cluster doped polyimide nanocomposite for the selective detection of carcinoembryonic antigen

P J Jandas[a], Jingting Luo[a,b]*, K. Prabakaran[a], Fu Chen[a]*, Yong Qing Fu[c]

[a]Key Laboratory of Optoelectronic Devices and Systems of Ministry of Education and Guangdong Province, College of Physics and Optoelectronic Engineering, Shenzhen University, 518060, Shenzhen, PR China

[b]State Key Laboratory of Powder Metallurgy, Central South University, Changsha, PR China

[c]Faculty of Engineering and Environment, Northumbria University, Newcastle upon Tyne, NE1 8ST, UK

Dr. Ponnath Janardhanan Jandas

Shenzhen Key Laboratory of Advanced Thin Films and Applications,

College of Physics and Energy,

Shenzhen University,

Pin: 518060, Shenzhen, PR China

Email: drjandasjanan@gmail.com

Abstract

Herein, presents a novel method for the preparation of a Love mode SAW biosensor for the selective detection of carcinoembryonic antigen (CEA) using a transuding polymer nanocomposite thin film based bioreceptor. Graphene oxide (GO) was synthesized using modified Hummer's method and flower-like MoS_2 nanoparticles were allowed to grow on the 2D layers GO. The rGO-MoS_2 was further used as a host for the synthesis of Au nanoparticles (AuNP) and the final three-component nano-cluster was introduced to the previously synthesized polyamic acid diethyl ethanolamine salt precursor. The uniform mixture was coated on the delay line area of SAW device and conducted thermal imidization process to obtain polyimide nanocomposite. The thickness of the thin film was optimized based on the insertion loss and centre frequency response of the SAW device. Further, anti-CEA self-assembled monolayer (SAM) based bioreceptor was prepared on the polyimide nanocomposite thin film through thioglycolic acid – EDC/NHS immobilization mechanism. The bioreceptor was tested for immunoassay analysis with CEA solution with varying concentrations. The LOD of the biosensor was estimated at 0.084 ng/ml. The real-time applicability of the biosensor was validated using clinical serum sample analysis and the selectivity was evaluated through the affinity test towards other common tumour marking proteins. The biosensor also showed excellent stability, only 10% reduction activity was observed till 80^{th} day of storage. The antigen-antibody adsorption parameters were also evaluated through Langmuir and Freundlich adsorption isotherms.

Keywords*: SAW, Biosensor, Polyimide, Nanocomposite, GO, MoS_2, AuNP*

1. Introduction

Nanomaterial incorporated conducting polymers have been gained attention from the researchers in recent years as transducing media for biosensing application [1-2]. Nanoscale metal oxides, noble metal doped metal oxides, carbon-based nanomaterials including graphene oxide and CNTs are the common nanomaterials used for this purpose [3-4]. The most widely investigated conducting polymers are polyaniline, poly(phenylenevinylene), polypyrrole, polyimides and polythiophenes [5-7]. Biosensors based on conducting polymer nanocomposites are highly sensitive due to the large surface to volume ratio of the nanostructure and shows excellent selectivity when coupled with bio-recognition molecules [8]. Nanoparticles can act like electron connector while, matrix polymer can assist selective adsorption of target analyte. This makes conducting polymer nanocomposite thin film as an efficient biosensing transducing electrode [9]. A thin layer of conducting polymer can act as a medium for biomolecular immobilization through electrochemical entrapment, covalent immobilization or affinity interactions [10]. Such immobilized biomolecules attract the analytes through adsorption process. This may end up as change in mass, optical activity, electrical conductivity and temperature around the electrode surface. Such changes can detect using a suitable detector. Many research reports are available on the bioreceptor applicability of conducting polymer-based nanocomposites as electrochemical, optical, calorimetric and piezoelectric biosensors [2].

In the present contest, we are particularly interested in piezoelectric sensors and more in specific, surface acoustic wave (SAW) biosensors due to its highly sensitive, real-time and label-free detection capability of biological macromolecules [11]. The popularity of SAW device is attributed to its compact size, low cost and easy data analysis as well [12]. SAW device finds application in the biosensing of living cells [13], protein-protein interaction study [14], analysis of single biomolecular structure [15] and detection of tumour marking proteins

[16]. Preparation of bioreceptor on the delay line area of SAW device is vital in case of biosensing of molecules with biological origin. The sensitivity, selectivity and stability of the SAW biosensor are greatly depending on the performance of the bioreceptor surface [17]. Various methods including chemical, inorganic thin film and nanoparticle-based immobilizations of bioreceptors are reported in various studies [18-19]. Bioreceptors can be prepared through polymer structures as well. Branch and Brozik have been studied on the effect of polyimide (PI) and polystyrene (PS) based bioreceptors for the biosensing of Bacillus anthracis stimulant and Bacillus thuringiensis [20]. Novolac polymer was used by Gizeli et al. for the immobilization of protein to biosence immunoglobulin G [21]. Dextran and polyethylene glycol were used for the detection of recombinant human (rh) HER-2/*neu* [22]. Ritter et al. were utilized polystyrene microparticles colloid crystals as a bioreceptor base for the protein detection [23]. Polyvinyl alcohol (PVA) and polyvinyl pyrrolidone (PVP) thin films also find as effective materials for the SAW bioreceptor preparation as a humidity sensor by Buvailo et al. [24].

In the present study, AuNP-MoS_2-rGO nano-cluster doped polyimide nanocomposite (PI/ AuNP-MoS_2-rGO) was synthesized and studied its application as a bioreceptor base for the selective detection of CEA for the first time. CEA is a tumour marking protein associated with various types of cancer in the body. Early detection of an abnormal concentration of CEA in the human body can be useful for the identification of tumour, understand the growth stage and suggest effective treatments [25]. Studies are available on the selective detection of CEA using SAW device. However, sensitivity, stability and selectivity of the biosensor still are the popular topics to ponder. We have chosen a conducting polymer-based bioreceptor in this perspective which can provide better stability to the SAW biosensor. However, polymer-based SAW devices have main drawback as high insertion loss and thereby low analysis window [21, 26]. To overcome such hurdles we have prepared conducting polymer nanocomposite system in

which the nanoparticles can act for better conduction/transduction of acoustic waves synergistically with the inherent properties of the matrix polymer [27-28]. rGO and MoS_2 are proven materials for the signal transduction for biosensing applications [29, 36-37]. Additionally, we have used AuNP within the nanocomposite as the reaction nuclei for the immobilization of anti-CEA as bioreceptor. SAW device was fabricated by photolithography method with double head interdigital transducers. The delay line was modified using PI/AuNP-MoS_2-rGO thin film. The polymer nanocomposite thin film was further converted as a bioreceptor through the immobilization of antibody of CEA (anti-CEA) via thioglycolic acid bridging using EDC-NHS activation. The AuNP can act as the host for thioglycolic acid bridging groups through the covalent linkage between the mercapto part and Au. The prepared bioreceptor was further used for immunoassay analysis using CEA solutions with varying concentrations from 0.1 ng/ml to 80 ng/ml. Repeatability and long term stability of the device also were evaluated. The selectivity of the biosensor was studied using samples of alpha-1-fetoprotein (AFP), cancer antigen 125 (CA125) and L-tryptophan. The real-time application of the biosensor was evaluated using clinical serum samples as well. The Langmuir and Freundlich adsorption isotherm was employed for additional validation of the capability of the biosensor.

2. Materials

N, N dimethylethanolamine (DMEA), pyrometallic dianhydride (PMDA), 4, 4'oxydianiline (ODA), N-methyl pyrrolidone (NMP), graphite flakes, $KMnO_4$, Na_2MoO_4 .$2H_2O$, thiourea, thioglycolic acid, ethyl-dimethyl-aminopropyl carbodiimide (EDC), N-Hydroxy Succinimide (NHS), human CEA, mouse monoclonal antibodies to human CEA (which is also used in the reference ELISA kit), L-Tryptophan, AFP, CA125 and all the common chemicals of analytical grade were purchased from Sigma Aldrich. The activity of the CEA was evaluated using ELISA tests before using the biosensor based immunoassay analysis. Bovine serum albumin

(BSA) was purchased from Sinopharm Chemical Reagent Co., Ltd. China and phosphate buffer solution (PBS, 0.01 M, pH 7.2) was obtained from Solarbio Science & Technology Co., Ltd. China. The removable chemical protective coating used for the IDTs, Protectapeel, was purchased from Spaylat International, UK. Clinical serum samples were provided by Second People's Hospital, Shenzhen, China.

3. Experimental

3.1. Preparation of SAW device

Single side polished ST-cut quartz crystal with 4 inch in diameter was used to prepare SAW devices in the present study. The centre frequency of the device was recorded at 120 MHz. The device was prepared with two IDTs at the ends using Au electrode with 150 nm thickness and 60 finger pairs. The delay line area was maintained at the exact middle of input and output IDTs (4mm from each side). The quartz substrate was cleaned using acetone, isopropyl alcohol, and deionised (DI) water, followed by drying under nitrogen flow prior to the device preparation. A negative UV photoresist (SU-8) was coated on the quartz substrate using spin coating method. The thickness of photoresist was maintained at about 2μm by adjusting spin coating speed at 2500 rpm for 60 seconds. After the coating the substrate quartz crystal was baked at 90°C for 90 minutes and then exposed to UV light source for 2 seconds. In the next stage the substrate was baked again for 30 seconds at 95°C and 80s at 102°C. Further, the substrate was treated with the developer solution for 40 seconds through immersion method. In the final stage the photoresist was removed by washing the substrate using acetone.

3.2. Synthesis of polyamic acid diethyl ethanolamine salt

Synthesis of polyamic acid (PAA) precursor has conducted through the conventional aromatic diamine - dianhydride reaction method as given in the scheme 1. 1:1 stoichiometric amount PMDA and ODA in NMP solvent have taken in 250 ml RB flask attached with an air condenser. The reaction mixture was stirred using a magnetic stirrer for 18 hours under an N_2

atmosphere and normal temperature. The PAA precursor was further modified to PAA diethyl ethanolamine salt (PAD) to provide additional polar sites to interact with the nanoparticles to be incorporated through the added pendant diethyl ethanolamine group. The conversion was conducted by allowing the PAA to interact with DMEA in an air condenser using NMP at 25°C for 45 minutes. The resultant yellowish viscous solution of the precursor solution was stored in 4°C.

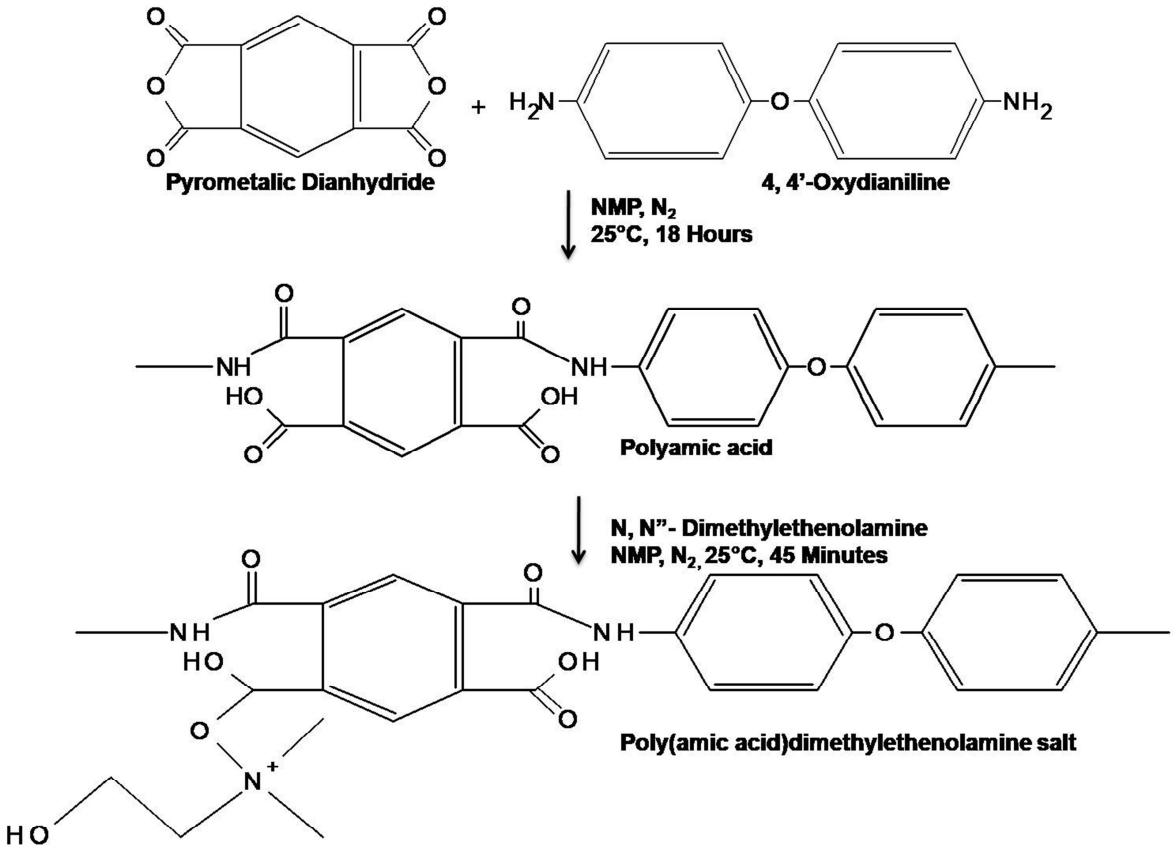

Scheme 1: Synthesis route for polyimide precursor

3.3. Synthesis of rGO doped with MoS_2 and AuNP

GO was synthesized using modified Hummer's method. A mixture of H_2SO_4 (36 ml) and H_3PO_4 (4 ml) was added carefully in an RB flask containing graphite flacks (0.3 g) and $KMnO_4$ (1.8 g). To avoid over heating due to the exothermic oxidation reaction, the RB flask kept in an ice bath. The temperature within the reaction mixture was maintained at 50±3°C

using a heater and kept under stirring for 12 hours. Further, the reaction mixture was cooled to room temperature and poured into 30% H_2O_2 solution in an ice bath. The precipitate was washed with deionised (DI) water and followed by 0.2 molar HCl. Finally, the GO obtained was washed with ethanol and diethyl ether. The GO flakes dried in a vacuum oven for 12 hours and stored.

0.4 g of Na_2MoS_2 .H_2O and 30 mg of GO was dispersed in 30 ml DI water with the help of ultrasonication in a 50 ml beaker. 0.63 g thiourea was added to the above reaction mixture and sonication was continued for 30 minutes. In the next step, the reaction mixture was transferred to a Teflon lined stainless steel autoclave and heated to 220°C using an electric oven for 24 hours. Further, it was cooled to room temperature and the resulting black precipitate of MoS_2-rGO washed with DI water and ethanol, followed by drying in a vacuum oven at 60°C.

0.05 g of MoS_2-rGO was taken in an RB flask containing 25 ml of DI water. The mixture was heated to 90°C and added 2.5 ml of 10.35 mg/ml of sodium citrate followed by 1 ml of 5 mg/ml aqueous solution of $HAuCl_4$ $3H_2O$. Heating continued for 15 minutes and the resulting solution cooled to room temperature using an ice bath. The precipitate of Au nanoparticle embedded MoS_2-rGO (AuNP-MoS_2-rGO) nano-cluster was filtered and washed with DI, followed by ethanol. Finally, the nanoparticles were dried in a vacuum oven at 80°C and stored at room temperature.

The nanoparticles were characterized using transmission electron microscope (TEM, Titan 3 Themis G2, ThermoFisher Scientific) and scanning electron microscope (SEM, Zeiss EVO-MA) images.

3.4. AuNP-MoS2-rGO/PI thin-film based SAM preparation

5 g of polymer precursor was mixed with 5 ml of DMAc and 0.15 g AuNP-MoS_2-rGO using sonication into uniform dispersion. Immediately after the sonication 10 μL of the nanocomposite mixture was placed on the delay line area (1 mm x 5 mm) of the SAW device

after covering the IDTs using removable protective coating, Protectapeel. The thin polymer nanocomposite film was made by a spin coating method, 10000 rpm for 60 seconds. The thin film further underwent stepwise thermal imidization in a vacuum oven at 120°C for 2 hours, 150°C for 2 hours and 180°C for 1 hour. Then present *in-situ* polymerization method is a novel path to prepare a bioreceptor on a piezoelectric substrate without using corrosive reagents like piranha solution and con. H_2SO_4. Various iterations of the reaction was conducted and optimized to maintain the thickness of the film of around 500 ± 25 nm. The device was conditioned in room temperature for 12 hours and cleaned using 1N HCl solution and finally with DI water. The delay lines of few of the SAW devices were further incubated with thioglycolic acid for 4 hours. After the removal of excess thioglycolic acid using DW, the delay line was treated with EDC and NHS for surface activation. The layer has further incubated with anti-CEA (100 μg/ml) for 4 hours and cleaned with DI water. The remaining unreacted NHS-esters were deactivated using 1 M ethanolamine, pH 8.0 solution and washed again with DI water. The bioreceptors prepared through this method was stored under sterile conditions at 4°C. The chemistry behind the immobilization process is given Scheme 2. The morphology of the bioreceptors was characterized using scanning electron microscope (SEM, Zeiss EVO-MA), atomic force microscope (AFM, Bruker NanoWizard®4 BioScience) and contact angle study(United Test Co., Ltd, CAG100 Contact Angle Goniometer).

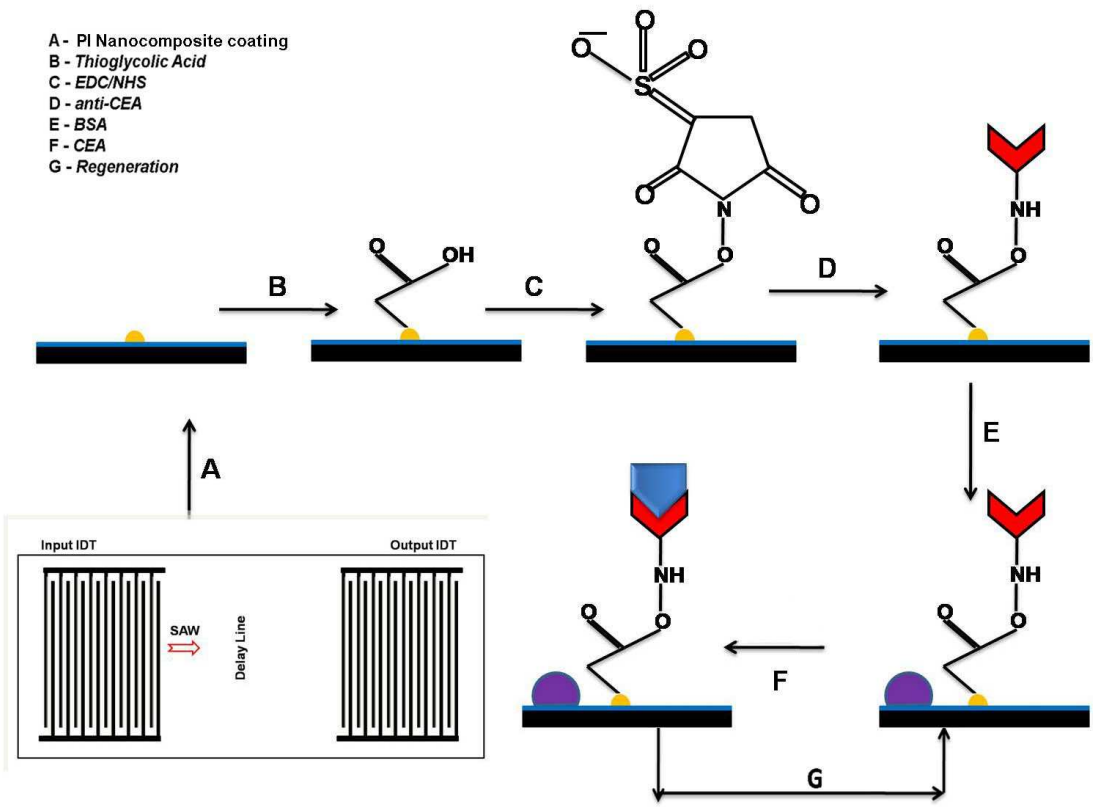

Scheme 2: Protocol followed for the anti-CEA immobilization on the delay line area of SAW device

3.5. Biosensing immunoassay analysis

A microfluidic chamber was prepared as given in Figure 1. The device has specially designed to connect with a 3 channel sample inlet system, contact points to SAW device and network analyser. The total analysis set-up was prepared as given in Figure 1. CEA solutions of concentrations ranging from 0.1 ng/ml to 80 ng/ml were used for immunoassay analysis to understand the biosensing capability of the biosensors. The immunoassay response in terms of change in centre frequency of the SAW device corresponding to the anti-CEA capture was recorded using a network analyser, Keysight Technologies, E5071C. An automated sample injection system was used to introduce a sample to the SAW biosensor placed in the micro-fluidic chamber. The flow rate was optimized at 0.05 ml/minute and each test was continued until the centre frequency reached an equilibrium plateau. Before exposing the biosensors to

CEA samples, treated with bovine serum albumin (BSA) to reduce the undesired adsorptions. A predetermined volume of CEA solutions prepared in the PBS was allowed to flow through the biosensor surface placed in the microfluidic chamber during each immunoassay analysis. Every sample was tested for minimum of 5 runs to evaluate the repeatability, reproducibility and estimate the standard deviation. At the end of each immunoassay measurement, the bioreceptor washed with PBS to understand the final equilibrium frequency shift. Further, a buffer solution containing HCl (0.8M), KCl (0.06M) and glycine 0.06M was used to regenerate the bioreceptor surface. Regeneration run was conducted until a stable plateau of centre frequency was obtained. Clinical serum samples were tested after optimizing the process of immunoassay analysis using known concentrations of CEA solutions. The selectivity of the SAW biosensor was tested using immunoassay analysis with a mixture of CEA and other common tumour marking proteins such as alpha-1-fetoprotein (AFP), cancer antigen 125 (CA125) and L-tryptophan. The stability of the SAW biosensor was tested as well. The device was stored at 4°C and 50 ± 5% relative humidity and tested for immunoassay analysis after every 5 days of intervals till 90 days.

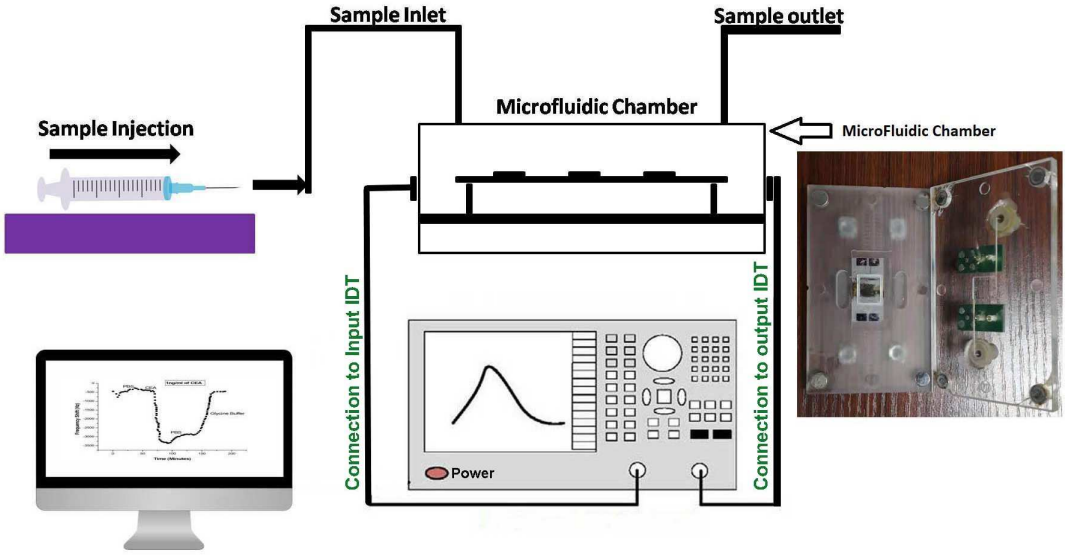

Figure 1: Biosensing set-up used in the present study

4. Results and Discussions

4.1. Synthesis of AuNP-MoS_2-rGO/PI

The successful conversion of graphite layers to AuNP-MoS_2-rGO nanoparticles was confirmed using morphological analysis. SEM imaging at various stages of the synthesis process was recorded and depicted in the Figure 2. The conversion of graphite to GO was conducted through modified Hummer's methods. We could record the images of single flacks of GO as given in figure 2. The layer has the longest cross-sectional length of 70 nm. Further, the MoS_2 nano-flowers were synthesized on the GO surface. The formation of MoS_2 on the rGO layer is visible in the figure, where the flattened surface represents the rGO layer and MoS_2 as the flower-like structure. The average diameter of well-formed flower-like MoS_2 molecules was recorded at around 20 nm. In the final step of hybrid nanomaterial synthesis, AuNP was allowed to form on the MoS_2-rGO structure and the resultant AuNP-MoS_2-rGO was imaged through SEM. The small spherical type particles of AuNP on the MoS_2-rGO surface are visible in the figure. The average size of these AuNP formed was measured around 6-10 nm. However, the distribution of these three nanomaterials was not well interpreted using SEM. In this view, additional evidence for the successful synthesis of the hybrid nanomaterial was collected through TEM imaging with elemental mapping.

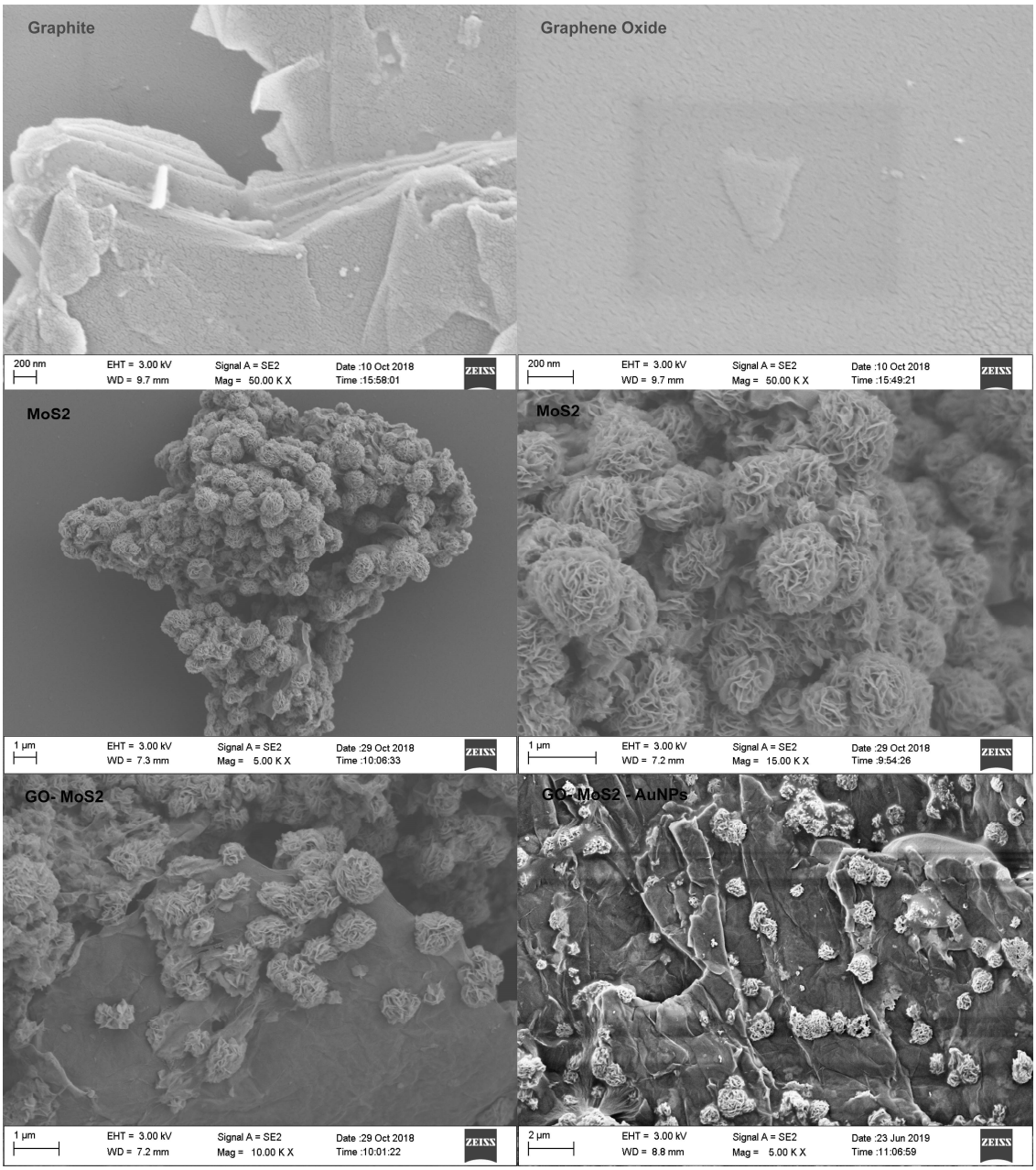

Figure 2: SEM images of graphite, GO, MoS_2, MoS_2-rGO and AuNP-MoS_2-rGO

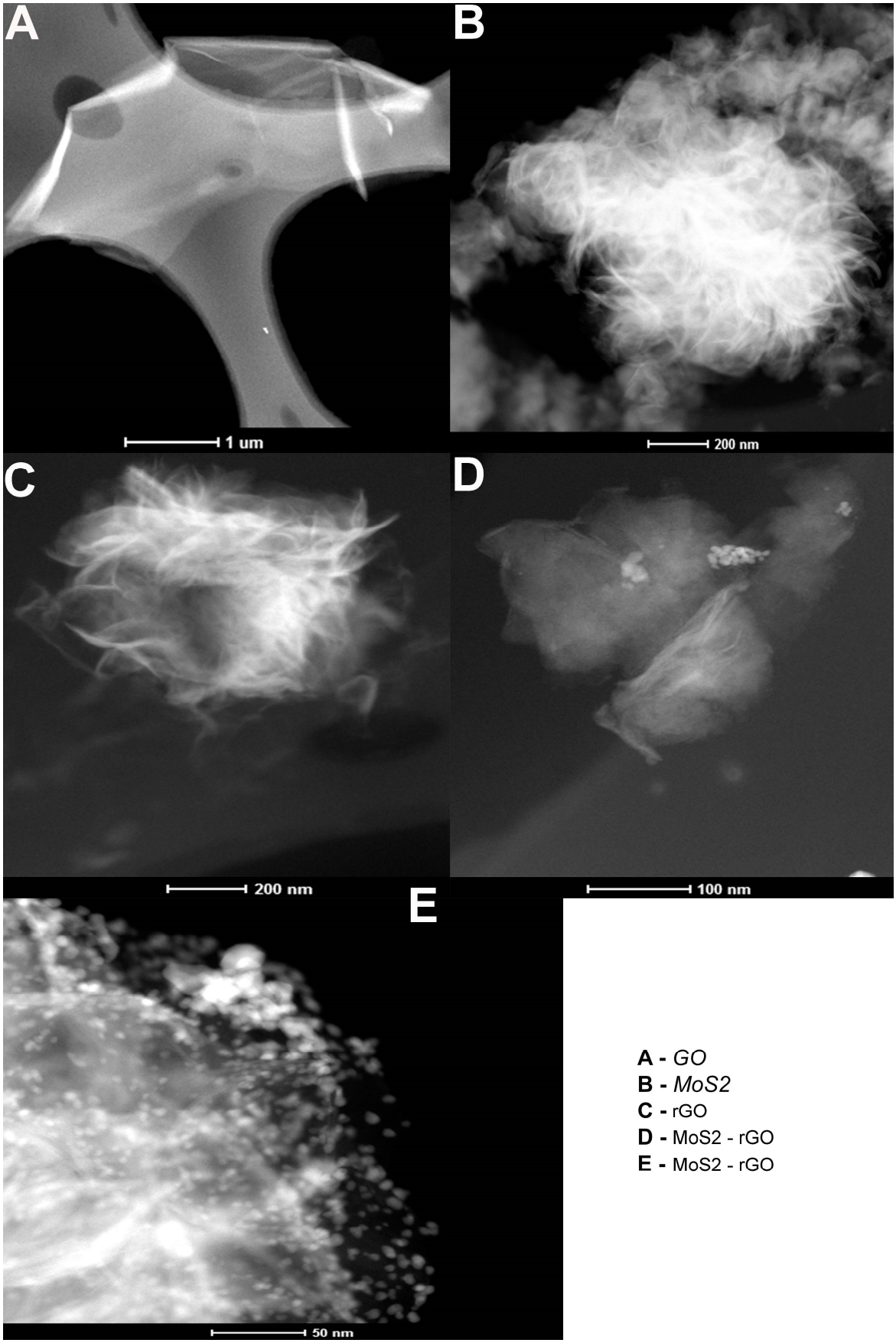

Figure 3: TEM images of graphite, GO, MoS_2, MoS_2-rGO and AuNP-MoS_2-rGO

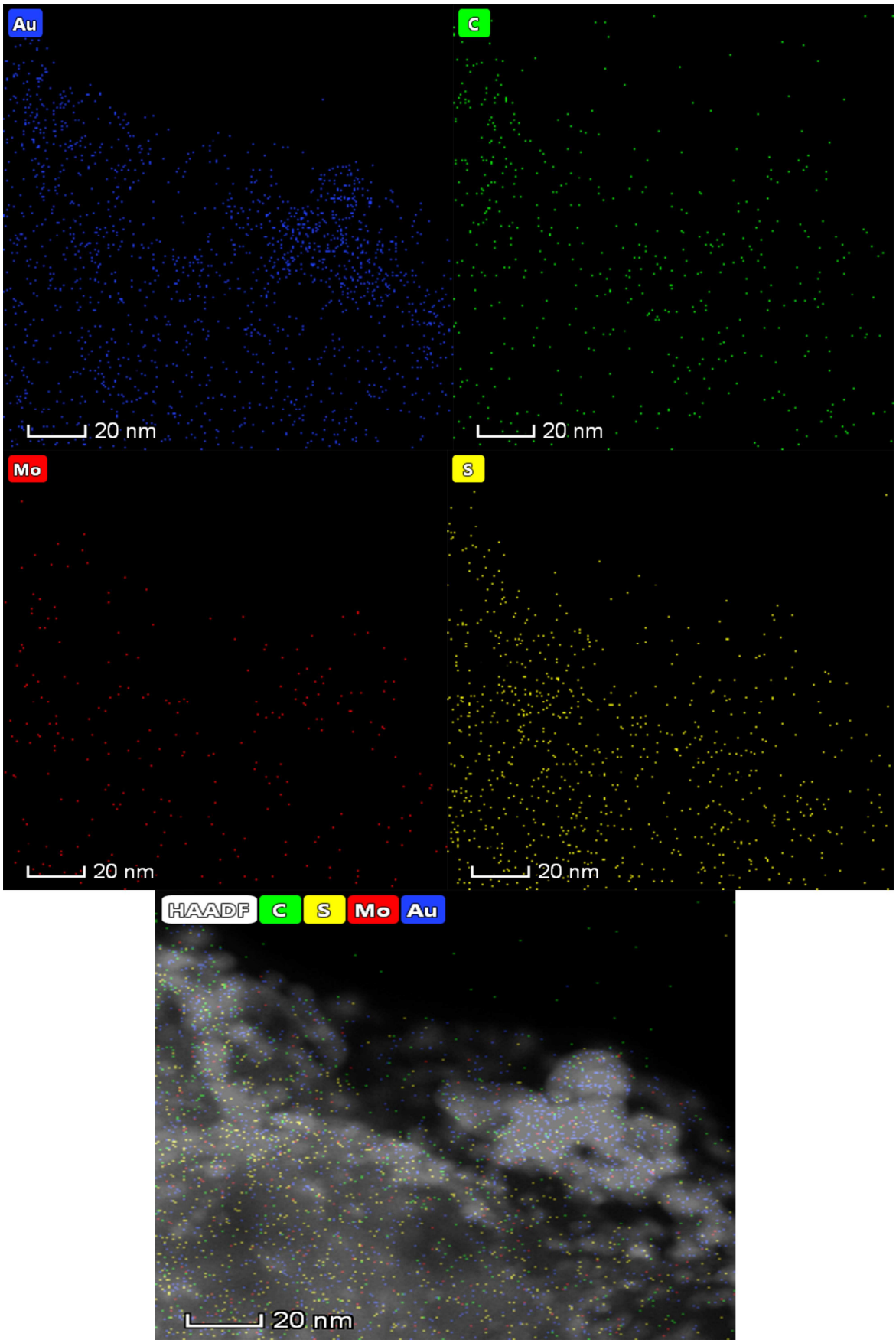

Figure 4: Elemental mapping of AuNP-MoS_2-rGO using TEM

Figure 3a-e represents the TEM images of GO, MoS_2-rGO and AuNP-MoS_2-rGO. The images of GO and MoS_2 has a comparable structure reported by previous studies [29, 30]. The thin layers of GO, the petals like parts of MoS_2 and the spherical AuNP are identifiable from the figures. However, to get a good insight into the formation of final hybrid nanomaterial elemental mapping was conducted and the results are given in figure 4. Since the material expected to be AuNP-MoS_2-rGO, the construction elements should be Au, Mo, C and S. Mapping was conducted for the aforementioned elements. Presence and uniform distribution of those elements are confirmed through the mapping and the analysis underlines the formation of AuNP-MoS_2-rGO hybrid nanoparticle. The elemental mapping also gives the idea about the uniform distribution of the nanoparticles which will be good for the formation of a stable, sensitive and consistent bioreceptor thin film as its polymer nanocomposite form.

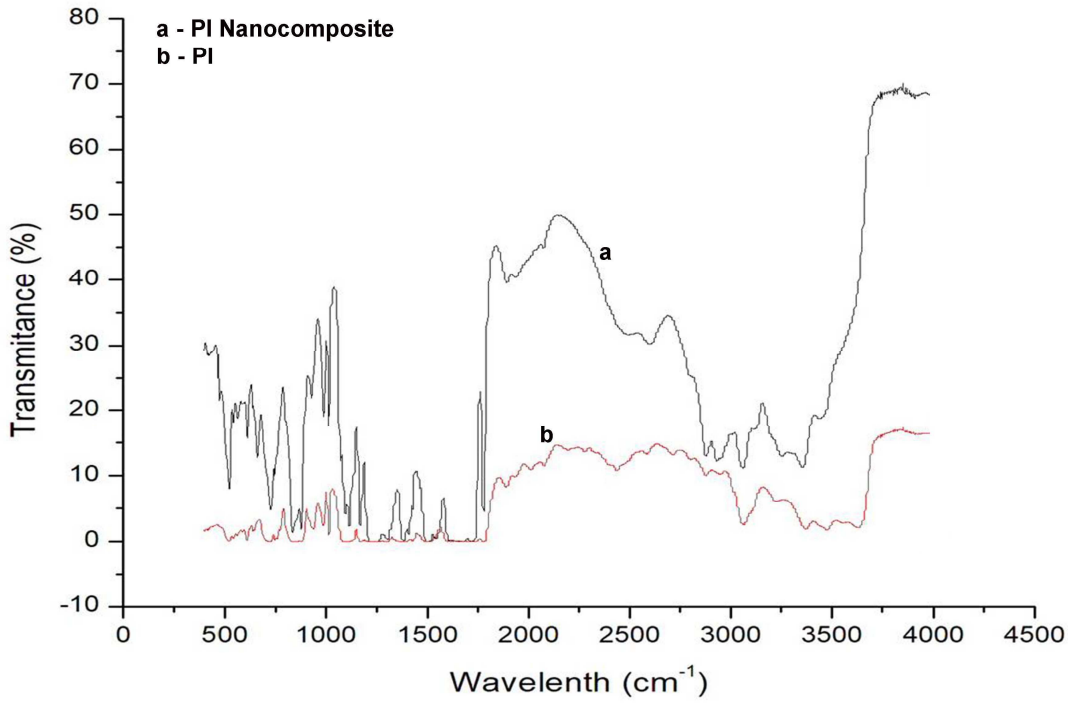

Figure 5: FT-IR spectra of PI and PI nanocomposites

The nanomaterial further incorporated within polymer precursor, coated on the delay line area of the SAW device and thermal imidization was conducted as discussed in the experimental

section. Formation of PI was confirmed using FT-IR spectroscopy and the spectra of PI and AuNP-MoS_2-rGO/PI are given in Figure 5. The characteristic imide C-N stretching frequency was identified in a region of 1300 cm^{-1}. The C=O stretching corresponding to carboxylic acid and ketone functionalities are noted around 1760 cm^{-1} and 1715 cm^{-1}. Further, aromatic C=C (m, m) vibration was identified at 1290 cm^{-1} as the confirmation of successful formation of PI. FT-IR spectra of PI nanocomposite also has taken and confirmed the incorporation of the nanomaterials did not make any change in the imidization process or macromolecular structure.

4.2. Bioreceptor preparation

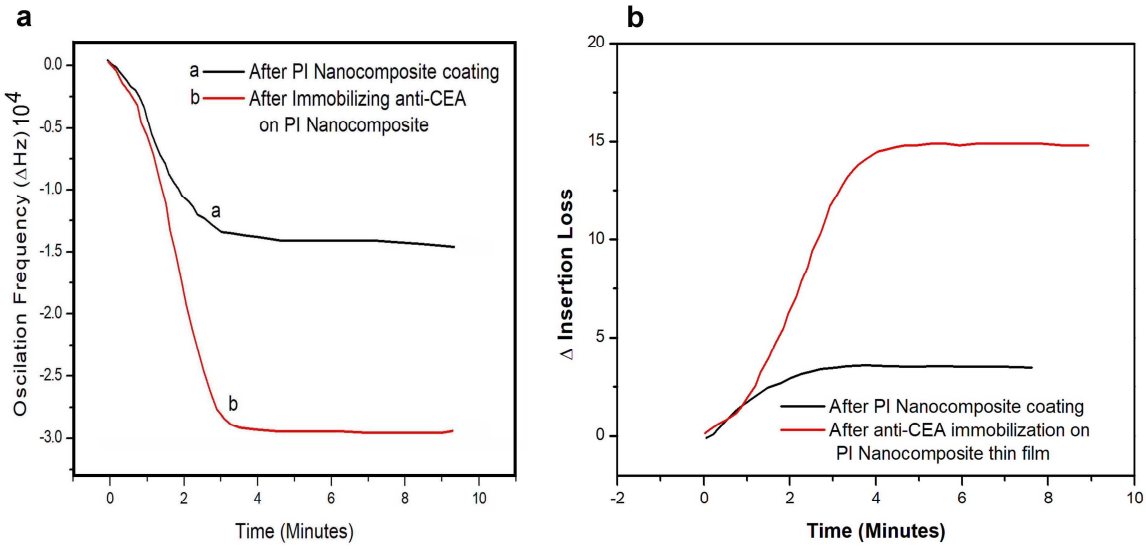

Figure 6: (a) Centre frequency shift during bioreceptor preparation (b) corresponding change insertion loss from the base value

The method of preparation of bioreceptor on the delay line area of SAW device is given in the Scheme 2. The AuNP-MoS_2-rGO/PI nanocomposite thin film was coated on the delay line and thioglycolic acid was allowed to interact with the AuNPs within the thin film. Mandana et al. were reported about the bioreceptor preparation on the Au coated SAW device [38]. However, the study has been used various chemical methods to trigger the sulphur – Au reaction. In the

present study, we have used a high surface to volume aspect ratio AuNP as the base, which can interact more effectively with the mercapto end of the thioglycolic acid than Au coated surface. Dense and uniform distribution of AuNP within the nano-cluster, which was identified through the TEM elemental mapping analysis, can lead to a uniform and stable base for the immobilization of anti-CEA. After each major step of bioreceptor preparation, the centre frequency response of the SAW device was recorded and the same is depicted in Figure 6.

The centre frequency response was recorded against PBS flow at a flow rate of 0.05 ml/minute. The base centre frequency has changed to a large extent after the polymer nanocomposite thin film coating on the SAW device as given in the figure 6a. The decrease in centre frequency can explain as when a SAW device is covered with the thin layer of dielectric material with less shear acoustic velocity than the piezoelectric substrate, the SH-SAW will convert to a guided wave known as the Love wave. For a specific frequency, three parameters including mass-loading (i.e. the mass of thin film deposited), the viscoelastic loading (i.e. the thin film viscosity and/or elastic properties) and electrical loading (conductivity of the thin film.) are the factors which affect the variation in centre frequency . In the present case, the comprehensive effect of these three parameters is expected to determine the final output of centre frequency and insertion loss. The thickness of the polymer nanocomposite thin film has maintained at 500 ± 25 nm through optimized spin coating parameters and after various trials. The data comprise of the relationship between the frequency shift, insertion loss and thickness of the thin film is given in the supportive data (Table S1).

The major concern for a polymer-coated bioreceptor on piezoelectric devices is large insertion loss after the coating of the thin film on the delay line area. This is due to the absorption of the acoustic wave by the polymer which has less shear acoustic velocity than the piezoelectric substrate. Also, the coating on the piezoelectric material may tend to generate surface skimming bulk wave, acoustic wave diffracts into the bulk of the crystal resulting in high loss

of energy [26]. However, in the present investigation, the intricacy was overcome through the use of the nanomaterial incorporated conducting polymer system, through which insertion loss was maintained in a minimum value after the thin film coating of SAW device. The insertion loss has shifted only by 3 dB after the polymer nanocomposite thin film coating. The base insertion loss of the SAW device was about 18 dB. The minimal increase in insertion loss value is pointing out about the support of AuNP-MoS_2-rGO/PI polymer nanocomposite for accosting wave conduction. Conducting polymers are poly-conjugated macromolecules with electronic properties comparable to metals along with retained properties of conventional organic polymers. Compared to saturated polymers, conducting polymers have the unique electronic pattern, low ionization potentials and high electron affinity [2]. The ground state Π-bonds of conducting polymers are assumed as partially localized due to a phenomenon called the Peierls distortion [5]. When conducting polymers doped with nanoparticles like graphene oxide, metal nanoparticles or oxides, the electronic excitation across the (Π – Π*) band gap creates self-localized excitation of conjugated polymers with localized electronic states in the gap region. These self-localized excitation known as polarons, bipolarons and solitons and provides easy conduction of electromagnetic waves [2]. However, the insertion loss was varied according to the thickness of the thin film. Based on the insertion loss and centre frequency response the thickness of the PI nanocomposite thin film was optimized at 500 nm. As given in the table, a further increase in thickness generates a sudden increase in insertion loss, which is not favourable for a highly sensitive biosensor. However, the complete formation of the bioreceptor (immobilization of anti-CEA), the insertion loss tends to increase by an additional loss of 12 dB. This is understandable since the thin film of biological molecules comprise of anti-CEA may absorb acoustic wave or create surface skimming bulk wave effect or a combination of both, thereby the corresponding increase in insertion loss and decrease in centre

frequency . The detailed analysis of the biological thin film of the bioreceptor was conducted through morphological imaging by SEM and AFM.

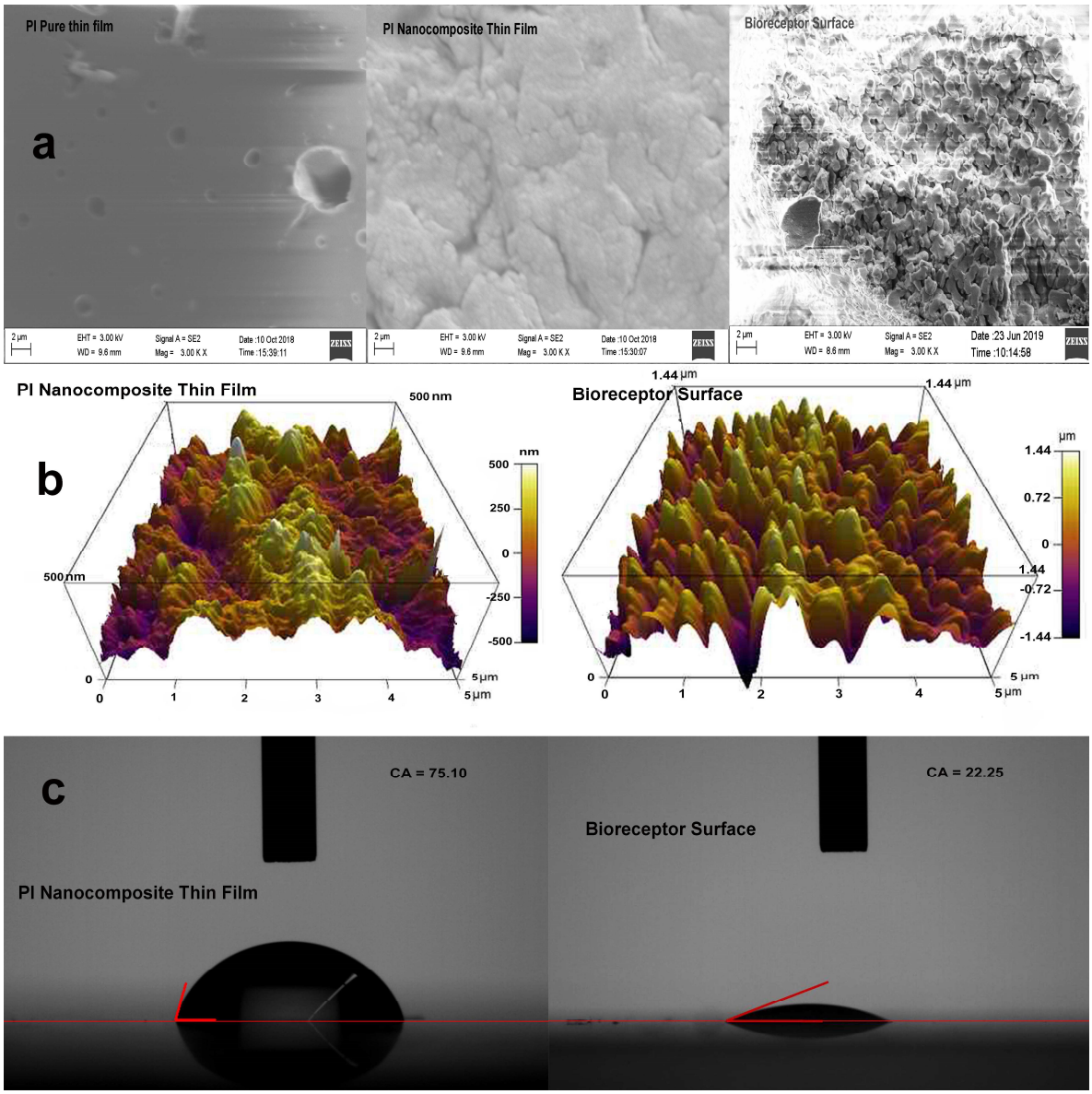

Figure 7: (a) SEM figures of bioreceptor (b) AFM figures of bioreceptor (c) contact angle of bioreceptor in comparison with PI nanocomposite thin film surface

The SEM images of the delay line area after the polymer nanocomposite coating and immobilization of anti-CEA are depicted in the Figure 7a. For a comparative purpose, the PI thin film morphology also is given in the figure. The pure PI surface was observed smooth, apart from some areas of depressions created by solvent trapping. The polymer nanocomposite

surface observed uneven throughout the surface, which is due to the presence of nanoparticles within the polymer matrix. This has modified in the case of bioreceptor, as a well-formed biofilm of anti-CEA changed the morphology to a properly distribute distinct textures throughout the delay line area as given in the figure. The AFM images further allowed understanding the dimensional details about the thin films formed on the SAW device, Figure 7b. The average thickness of the AuNP-MoS_2-rGO/PI thin film was observed as ~500 nm and the total thickness of the bioreceptor was reported as 1300-1400 nm. The polymer nanocomposite surface is observed with rough pillars owing to the presence of nanoparticles within the PI matrix. However, the added thickness on the surface after the anti-CEA immobilization further tends to increase surface roughness. The variation in the surface thickness was observed around 800 - 900 nm before and after the bioreceptor preparation. The increased thickness within the above-stated range also pointing out that the addition is a monolayer of anti-CEA as bioreceptor [39]. In addition to this, the successful formation of bioreceptor also confirmed using contact angle measurement of the delay line area. The contact angle was measured before and after the preparation of biofilm on the polymer nanocomposite thin film. Figure 7c, clearly suggests a huge difference in the contact angle of the surface before and after the anti-CEA immobilization. The value was changed from 75° to 22° due to the presence of hydrophilic glycoprotein anti-CEA biomolecules. The polar centres of the anti-CEA molecules can attract water molecules so that the contact angle of the delay line was abruptly reduced to a smaller value.

4.3. Immunoassay analysis of the biosensor

The immunoassay analysis was conducted using various concentrations of CEA samples ranging from 0.05 ng/ml to 80 ng/ml to understand the upper and lower limit of the newly prepared biosensor. The results were recorded as the change in the centre frequency of the SAW device w.r.t the concentration of analyzed CEA sample. The successful adsorption of

CEA molecules on the bioreceptor surface expected to reduce the centre frequency of the acoustic wave. A practical lower limit of 0.1 ng/ml was obtained since the biosensor didn't respond to the CEA solution beyond this concentration. The upper limit of saturation was observed after 80 ng/ml of CEA sample solution. As discussed in the experimental section multiple immunoassay runs were conducted for each CEA sample with a specific concentration and mean value of centre frequency difference was calculated and used to characterize the biosensor. One example of such response observed for each concentration (0.1 to 80 ng/ml) is depicted in Figure 8a, also the cycle of analysis is given in 8c. Figure 8b represents the average values of overall analysis conducted for each concentration and Figure 8d is the log-log calibration plot for the biosensing analysis conducted. The centre frequency changes linearly with the change concentration of CEA solution. The biosensor was responded with a frequency difference (Δf) of around 150 Hz from the base bioreceptor frequency against the 0.1 ng/ml of CEA sample solution. Further, the shift in centre frequency has given a linear decrease with the increase in w.r.t the concentration of CEA and a corresponding linear increase in the difference in centre frequency from the based value of the bioreceptor. The limit of detection of the biosensor was calculated at 0.084 ng/ml using the following formula, LOD = 3 x σ/Sensitivity [31]. The regression coefficient (R^2) was calculated as 0.9778. The average values of centre frequency response were compared with an Au coated SAW biosensor and results are given in the supportive data (table S2). The sensitivity in terms of centre frequency response found much larger for the present biosensor as compared to the Au coated SAW device based biosensor. Better exposure of the high aspect ratio Au nanoparticles on the PI nanocomposite thin film creates many numbers of reaction sites than Au coated surface. Additionally, better transduction and conduction acoustic wave through the conducting polymer-based nanocomposite system also contributed to the better response to the antigen-antibody reaction. Such a synergistic effect ultimately leads to the one of the least value of

LOD for the present biosensor among the various piezoelectric biosensors reported for CEA detection. The LOD values are compared with the other reported piezoelectric biosensors for CEA and given as Table S3. The efficiency of the biosensor was also evaluated by comparing the experimentally deposited mass of CEA on the biosensor during each immunoassay analysis with total mass of CEA molecules flowed (theoretical) through the device. Theoretical values calculated by estimating the overall volume of a known concentration of CEA solution flown through a biosensor for a fixed time period. The deposited mass on the biosensor in real during immunoassay analysis was calculated as per the method suggested by Li et al. [31]. The results are given in Table 1 and the experimentally measured data is in good agreement with the theoretical values.

Table 1: Comparison of the experimentally calculated deposited mass on the biosensor with theoretical values

The concentration of CEA stock solution (ng/ml)	**Experimental value (ng)**	**Theoretically calculated value (ng)**
0.1	0.26±0.03	0.3
0.5	1.31±0.15	1.5
1	2.81±0.16	3
5	14.16±0.5	15
10	26.9±2.4	30
20	56.45±2.8	60
30	84.5±4.5	90
40	117.45±2.6	120
50	148.6±1.0	150
60	175.1±3.8	180

70	204.5±5.1	210
80	235.2±3.6	240

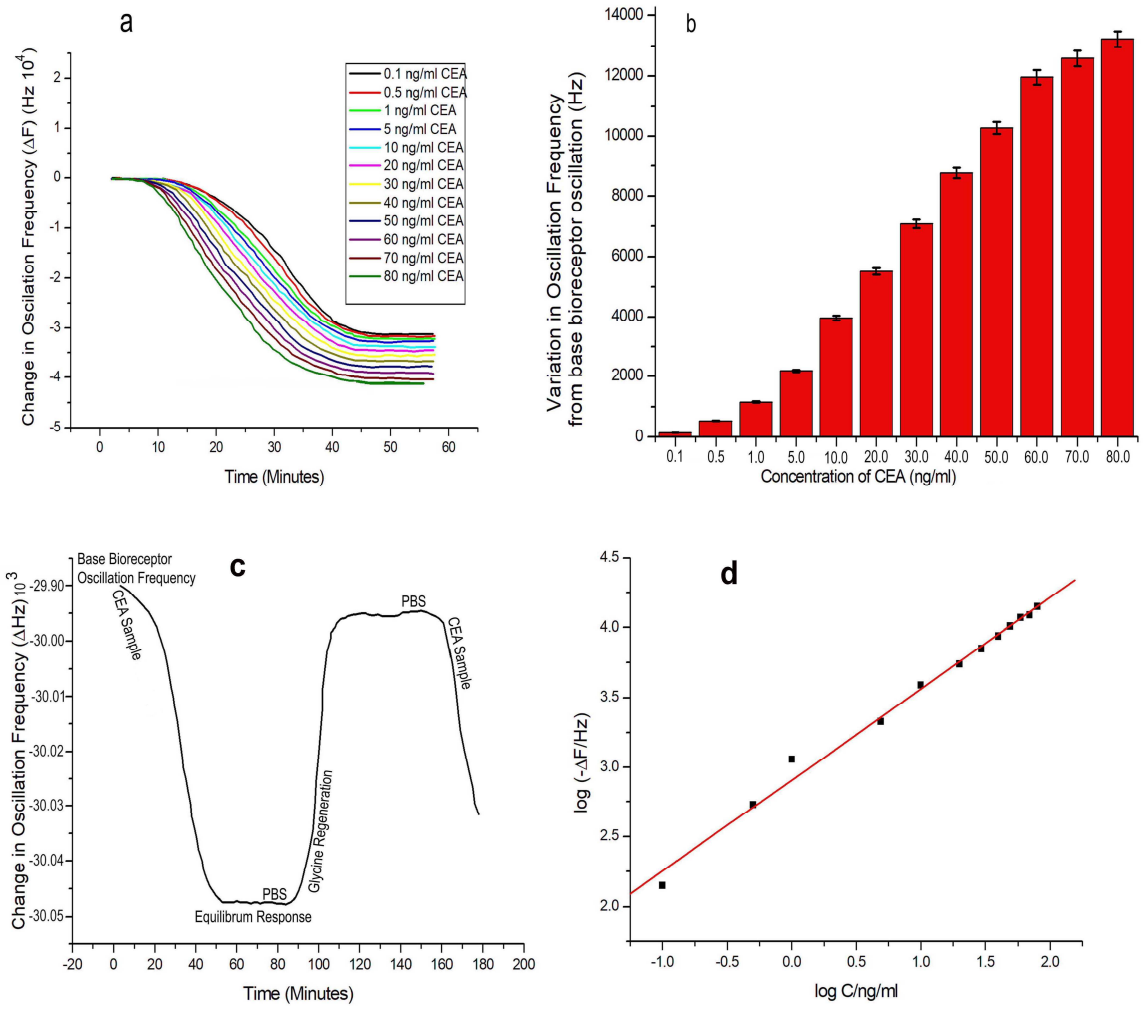

Figure 8: (a) immunoassay response of the biosensor to various concentrations of CEA (b) Variation of centre frequency from the base frequency for each concentration of CEA (c) centre frequency shift during the cycle of analysis (d) log-log calibration plot for the present set of analysis

The adsorption parameters to understand the CEA interaction with the anti-CEA at the bioreceptor interface can be evaluated through Langmuir and Freundlich isotherms, [32, 33]. Langmuir adsorption isotherm is stated as,

$C_e/q_e = (1/q_0b) + (C_e/q_0)$

C_e - Equilibrium concentration (mg/L) of CEA stock solutions,

qe - Equilibrium sorption capacity (mg mg^{-1})

q_0 - Indicates the real sorption capacity (mg mg^{-1}) of the biosensor

b - Measure of energy of sorption (L $mmol^{-1}$).

The quantity of the constant values is taken from the available literature [32, 33].

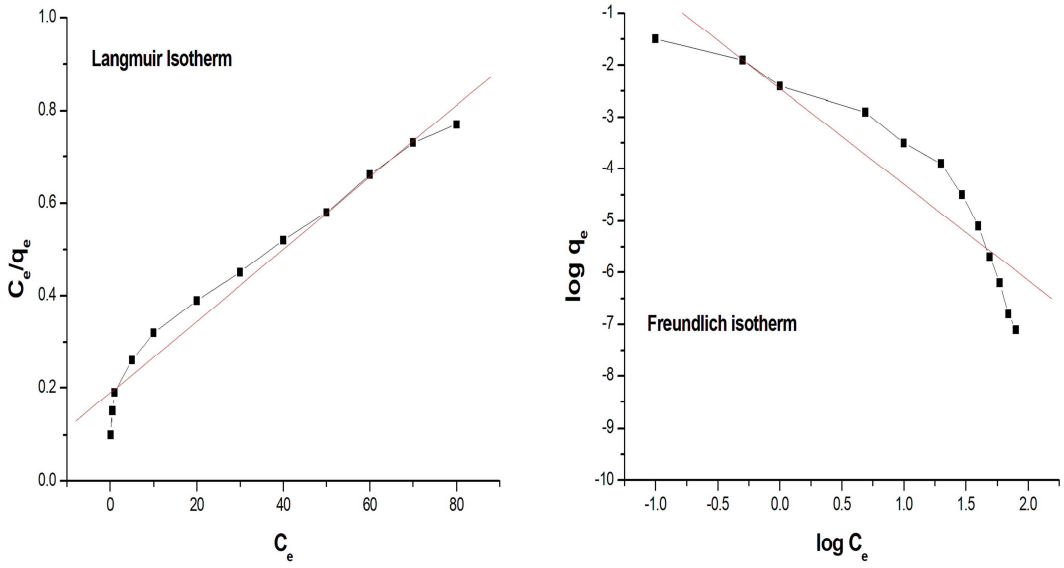

Figure 9: Langmuir and Freundlich adsorption isotherms

The isotherm curves were plotted as C_e/q_e v/s C_e and given in Figure 9. The slop and intercepts were calculated to be 2.37 mmol/g and 2.89 L $mmol^{-1}$ respectively. The values represent the adsorption capacity and the energy of adsorption of CEA on the antibody bioreceptor respectively. Also based on the data from the isotherm kinetic constants of adsorption (k_a) and desorption (k_d) were calculated as 3124 ± 874 L mol^{-1} s^{-1} and 7.43 ± 1.28) × 10^{-4} s^{-1} [34]. The dissociation constant was calculated as a non-zero value, which suggests an existing equilibrium within the interface of A-CEA – CEA during the immunoassay analysis. Additionally, the free energy of adsorption ($\Delta G_{sorption}$) was calculated as well at -6.3 ±0.81 kcal

mol^{-1}, which is a comparable value with the previous analysis reported for a favourable adsorption process [34].

Freundlich adsorption isotherm is the modified form of Langmuir isotherm which seemed to be more appropriate to define the liquid state biomolecular interaction parameters [33]. According to Freundlich adsorption isotherm,

$ln\ q_e = \ln K_f + (1/n)\ ln\ C_e$

K_f - Constant represents the adsorption capacity

n - Intensity of adsorption process

The isotherm was plotted as $\ln q_e$ v/s $\ln C_e$ (figure 9), isotherms suggest the sorption process of CEA on the anti-CEA bioreceptor follows Freundlich adsorption isotherm in a better way than the Langmuir. The adsorption capacity at 0.612 and the intensity of adsorption at 3.54 was calculated respectively as slop and intercept of the isotherm. The dimensionless constant separation factor "R_L" also can be calculated through Freundlich isotherm parameters which can give insight to the favourability of the adsorption process on the present bioreceptor interface during the immunoassay analysis. "R_L," value can be obtained as [34],

$R_L = 1/(1 + xC_0)$, "x" is termed as the energy or the intensity of the sorption process. The isotherm fit is the major factor to determine the value of R_L. More the linearity better will be the possibility to undergo the adsorption process.

$R_L > 1$, Adsorption termed as unfavourable

$R_L = 1$, linear

$0 < R_L < 1$, favourable

$R_L = 0$, irreversible.

In the present study, the R_L value was calculated as 0.904 which suggests a favourable adsorption process according to the concept. Overall both the isotherms parameters suggested a favorable adsorption conditions for CEA on the anti-CEA based bioreceptor.

4.4. Analysis of clinical serum samples

The real-time analysis ability of the biosensor prepared in the present study was evaluated through clinical serum sample analysis. The analysis was conducted with the support of the Second People's hospital, Shenzhen China. Hospital has provided 15 serum samples and the samples were collected and analyzed as a part of preliminary examination for colorectal cancer diagnosis. The samples were analyzed using the biosensor as well as the regular analysis, ELISA method. The samples for analysis were prepared by adding 0.5 mL serum in 2 mL of PBS solution with a pH value of 7.4. Results from both the analysis method are depicted in Table 2. According to the results, only 4 samples were suspected to contain an abnormal amount of CEA concentration. Sample number 1, 4, 5 and 15 have CEA concentration of 28.56, 37.63, 29.91 and 36.58 ng/ml respectively. Another two samples (11 and 12) with a marginally higher concentration than normal average values were reported at 12.74 and 13.61 ng/ml. In this view, the above mentioned 6 samples were suggested for further detailed analysis. The results obtained from the present biosensor are in good agreement with the results obtained through the ELISA method. The major advantages of the biosensor analysis are the consistency in the results and time of analysis. The standard deviations obtained for biosensor analysis are smaller than that of ELISA method. The time of analysis found way better than ELISA as the later took an average of 6-8 hours where the biosensor analyzes within 40-60 minutes.

Table 2: Validation of the biosensor using clinical serum sample analysis

Sample No.	SAW Biosensor results (ng/ml)	ELISA (ng/ml)
1	28.56±2.26	28.93 ±4.16
2	2.52±0.38	2.67 ±0.57
3	4.68±0.28	4.91 ±0.46

4	37.63±2.16	38.03 ±4.52
5	29.91±3.79	29.51 ±5.68
6	3.39±0.23	3.48 ±0.44
7	4.73±0.38	4.58 ±0.59
8	3.77±0.21	3.93 ±0.48
9	4.76±0.35	4.99 ±0.51
10	2.18±0.15	2.48 ±0.46
11	12.74±1.36	13.20 ±2.73
12	13.61±1.85	13.31 ±4.33
13	4.35±0.54	4.52±1.22
14	4.35±0.58	4.52±1.31
15	36.58±3.34	36.89±5.61

4.5. The selectivity of the biosensor

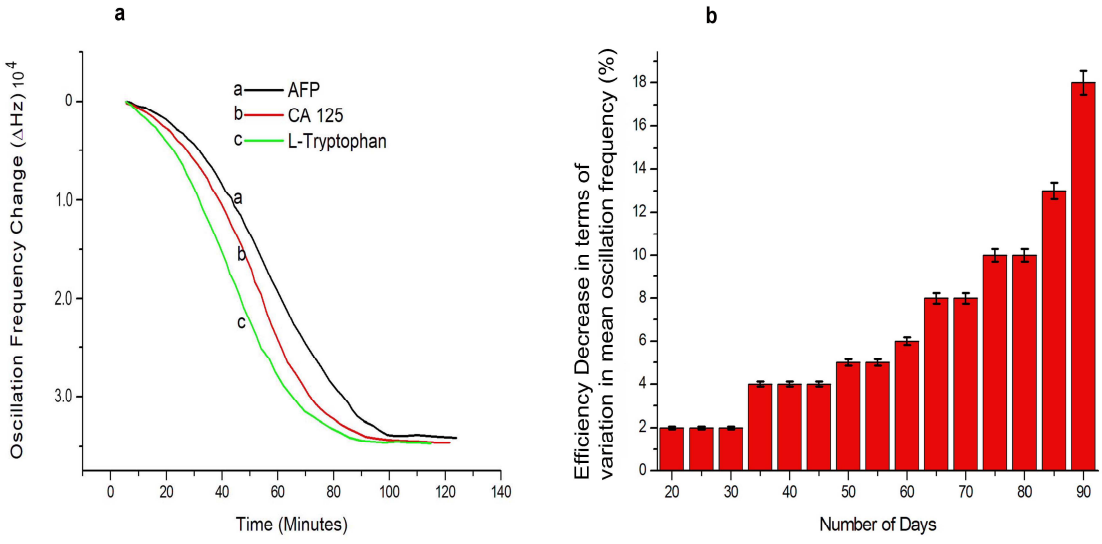

Figure 10: Selectivity analysis of the biosensor (b) stability study of the biosensor

The selectivity analysis of the biosensor was conducted through the immunoassay analysis of CEA in the presence of some of the other common tumour marking proteins. We have opted three protein molecules including alpha-1-fetoprotein (AFP), cancer antigen 125 (CA125) and L-tryptophan for this study. Various combinations of these samples were prepared as given in the Table S4 and immunoassay runs were conducted. A representative image of selectivity analysis sample numbers 4, 5 and 6 is given in Figure 10a. According to the results, the biosensor didn't show any considerable affinity towards the other tumour marking proteins. The equilibrium frequency shift obtained for each immunoassay run was within the range obtained from the pure CEA solution. The results suggest the prepared biosensor has a good selectivity towards CEA tumour marking proteins and it has a negligible affinity on the other tumour proteins.

4.6. Long term stability of the Biosensor

The storage capability and long term applicability of the biosensor were evaluated for 90 days. A batch of 10 PI nanocomposite based biosensors was used for this study and the immunoassay evaluation was conducted at every 5 days of intervals to understand the consistency in the results. The samples were stored in sterile conditions at 4°C after each immunoassay analysis. The average value of biosensing performance in terms of centre frequency shift was estimated in comparison with the initial day value. The percentage of decrease in a frequency shift of the immunoassay response is depicted in the Figure 10b. The biosensor did not show any considerable variation in the results within a period of 25 days. Within this period the variation in centre frequency decrease was only up to 3%. The PI nanocomposite thin film can provide a stable platform for the formation of receptor which ultimately results in high stability for the bioreceptor in addition to the high sensitivity towards CEA molecules. Further, till 65^{th} day a maximum of 7% variation was observed and at the end of the analysis period, 90^{th} day the variation was estimated at around 13%. A comparative study of stability conducted using

biosensor prepared on gold-coated delay line is given in the supportive data Table S5. The gold coated biosensors reported around 25% variation in the centre frequency response at around 35^{th} day and become unresponsive after 40^{th} day.

5. Conclusion

A novel polymer nanocomposite thin film was synthesized using PI, rGO, MoS_2 and AnNP and successfully utilized the thin film as a transuding bioreceptor base for the preparation of a liquid state love mode SAW biosensor for the selective detection of CEA. The PI nanocomposite thin film was coated on the delay line area of the SAW device specifically prepared for this study through photolithography method using an AT quartz crystal. Conducting polymer-based nanocomposite system has well supported to overcome the usual hurdle of high insertion loss for polymer-based SAW analysis. The inherent quality of the conducting polymers, rGO and MoS_2 have allowed the passage of love wave from the input to output IDT through the polymer nanocomposite coated delay line of SAW device without much loss in intensity. A maximum change in insertion loss of 3 dB was optimized for PI nanocomposite coating. Further, the bioreceptor of a self-assembled monolayer of anti-CEA was prepared via thioglycolic acid – EDC/NHS mechanism. The high aspect ratio AuNP's were acted like active reaction sites for thioglycolic acid attack and facilitate the formation of a dense biofilm of anti-CEA monolayer on the PI nanocomposite thin film. This ultimately results in a positive effect on the sensitivity and stability of the biosensor. The biosensor was validated for CEA sensing using a specially designed sample micro-fluidic system and a network analyzer. The biosensor has recorded a limit of detection value at 0.084 ng/ml and upper saturation point of 80 ng/ml of CEA concentration. With the support of good transduction capability of MoS_2 and rGO coupled with PI conducting polymer, the sensitivity in terms of variation in centre frequency w.r.t the base frequency of the bioreceptor was reported excellent for each sample of CEA. The biosensor has reported excellent selectivity

towards CEA and showed the least affinity towards the common tumour marking proteins like AFP, CA 125 and L-tryptophan. One of the most notable outcomes of the present study other than LOD is the exceptional stability of the present biosensor. The biosensor exhibited stable performance over 70-80 days without reporting much decrease in biosensing performance. The adsorption parameters like K_a and K_d were calculated as 3124 ± 874 L mol^{-1} s^{-1} and 7.43 ± 1.28) × 10^{-4} s^{-1} respectively using Langmuir adsorption isotherm. The nonzero K_d value has suggested the existing equilibrium between the forward and backward reaction. The free energy of adsorption was estimated as -6.3 ±0.81 kcal mol^{-1}, which also suggests a favourable condition for antigen-antibodydy interaction. The findings were further confirmed using Freundlich adsorption isotherm as well.

Acknowledgement

The authors gratefully acknowledge the support of Research and Development Program of China (Grant no. 2016YFB0402705), Project supported by State Key Laboratory of Powder Metallurgy, Central South University, Changsha, China, National Natural Science Foundation of China (NSFC Grant no. 11704261, 11575118), Shenzhen Science & Technology Project (Grant no. JCYJ20170817100658231, JCYJ20180507182439 57，JCYJ20180305124317872), Natural Science Foundation of SZU (Grant no. 2017067), Shenzhen Key Lab Fund (ZDSYS20170228105421966), UK Engineering and Physical Sciences Research Council (EPSRC) EP/P018998/1, Newton Mobility Grant (IE161019) from the UK Royal Society and the National Natural Science Foundation of China, and Royal Academy of Engineering UK-Research Exchange with China and India.

Conflict of interest

The authors do not have any conflict of interest regarding this publication.

References

1. Swati Shrivastava, Nimisha Jadon, Rajeev Jain, Next-generation polymer nanocomposite-based electrochemical sensors and biosensors: A review, TrAC Trends in Analytical Chemistry, 82, 2016, 55-67.
2. Mama El Rhazi, Sanaa Majid, Miloud Elbasri, Fatima Ezzahra Salih, Larbi Oularbi, Khalid Lafdi, Recent progress in nanocomposites based on conducting polymer: application as electrochemical sensors, International Nano Letters, 8, 2018, 79–99
3. Paolo Bollella, Giovanni Fusco, Cristina Tortolini, Gabriella Sanzò, Gabriele Favero, Lo Gorton, Riccarda Antiochia, Beyond graphene: Electrochemical sensors and biosensors for biomarkers detection, Biosensors and Bioelectronics, 89, 2017, 152-166,
4. hristopher B. Jacobs, M. Jennifer Peairs, B. Jill Venton, Review: Carbon nanotube based electrochemical sensors for biomolecules, Analytica Chimica Acta, 662, 2, 2010, 105-127
5. Saniye Soylemez, Serife O. Hacioglu, Melis Kesik, Hande Unay, Ali Cirpan, Levent Toppare, A Novel and Effective Surface Design: Conducting Polymer/β-Cyclodextrin Host–Guest System for Cholesterol Biosensor, ACS Appl. Mater. Interfaces, 2014, 6, 20, 18290-18300
6. Hurija Dzudzevic Cancar, Saniye Soylemez, Yeliz Akpinar, Melis Kesik, Seza Göker, Gorkem Gunbas, Murvet Volkan, Levent Toppare, A Novel Acetylcholinesterase Biosensor: Core–Shell Magnetic Nanoparticles Incorporating a Conjugated Polymer for the Detection of Organophosphorus Pesticides, ACS Appl. Mater. Interfaces, 2016, 8, 12, 8058-8067
7. Ahu Arslan, Senem Kıralp, Levent Toppare, Ayhan Bozkurt, Novel Conducting Polymer Electrolyte Biosensor Based on Poly(1-vinyl imidazole) and Poly(acrylic acid) Networks, Langmuir, 2006, 22, 6, 2912-2915

8. Lin Lu, Zhiwei Zhu, Xianqiao Hu, Hybrid nanocomposites modified on sensors and biosensors for the analysis of food functionality and safety, Trends in Food Science & Technology, 90,2019, 100-110
9. Pan Zhang, Tingting Sun, Shengzhong Rong, Dongdong Zeng, Hongwei Yu, Ze Zhang, Dong Chang, Hongzhi Pan, A sensitive amperometric AChE-biosensor for organophosphate pesticides detection based on conjugated polymer and Ag-rGO-NH2 nanocomposite, Bioelectrochemistry, 127, 2019, 163-170
10. A. Mohamed Azharudeen, R. Karthiga, M. Rajarajan, A. Suganthi, Fabrication, characterization of polyaniline intercalated NiO nanocomposites and application in the development of non-enzymatic glucose biosensor, Arabian Journal of Chemistry, 2019, doi.org/10.1016/j.arabjc.2019.06.005
11. Petr Skladal, Piezoelectric biosensors, Trends in Analytical Chemistry, 79 (2016) 127-133
12. Kerstin Länge, Florian Bender, Achim Voigt, Hui Gao, Michael Rapp, A Surface Acoustic Wave Biosensor Concept with Low Flow Cell Volumes for Label-Free Detection,Analytical Chemistry 2003, 75, 20, 5561-5566
13. Antonis Kordas, George Papadakis, Dimitra Milioni, Jerome Champ, Stephanie Descroix, Electra Gizeli, Rapid Salmonella detection using an acoustic wave device combined with the RCA isothermal DNA amplification method, Sensing and Bio-Sensing Research 11 (2016) 121–127
14. Laurent Fertier, Marc Cretin, Marc Rollanda, Jean-Olivier Durand, Laurence Raehm, Rémi Desmet, Oleg Melnyk, Céline Zimmermann, Corinne Déjous, Dominique Rebière, Love wave immunosensor for antibody recognition using an innovative semicarbazide surface functionalization, Sensors and Actuators B 140 (2009) 616–622

15. Xiang Liu, Jia-Ying Wang, Xiao-Bing Mao, Yong Ning, Guo-Jun Zhang, Single-Shot Analytical Assay Based on Graphene-Oxide-Modified Surface Acoustic Wave Biosensor for Detection of Single-Nucleotide Polymorphisms, Analytical Chemistry 2015, 87, 18, 9352-9359
16. H.P. Chan, C. Lewis, P.S. Thomas, Exhaled breath analysis: novel approach for early detection of lung cancer, Lung Cancer 63 (2009) 164–168.
17. Zhangliang Xu, Yong J. Yuan, Implementation of guiding layers of surface acoustic wave devices: A review, Biosensors and Bioelectronics 99 (2018) 500–512
18. Fayçal Hadj-Larbi, Rafik Serhane, Sezawa SAW devices: Review of numerical-experimental studies and recent applications, Sensors and Actuators A: Physical, 292, 2019, 169-197
19. Qiaozhen Zhang, Tao Han, Jing Chen, Weibiao Wang, Kenya Hashimoto, Enhanced coupling factor of surface acoustic wave devices employing ScAlN/diamond layered structure with embedded electrodes, Diamond and Related Materials, 58, 2015, 31-34
20. Darren W Branch, Susan M Brozik, Low-level detection of a Bacillus anthracis simulant using Love-wave biosensors on 36°YX LiTaO3, Biosensors and Bioelectronics, 19, 8,2004, 849-859.
21. E. Gizeli, F. Bender, A. Rasmusson, K. Saha, F. Josse, R. Cernosek, Sensitivity of the acoustic waveguide biosensor to protein binding as a function of the waveguide properties, Biosensors and Bioelectronics 18 (2003) 1399_/1406
22. Friederike J. Gruhl, Kerstin Länge, Surface modification of an acoustic biosensor allowing the detection of low concentrations of cancer markers, Analytical Biochemistry 420 (2012) 188–190

23. F. Ritter, J. Hedrich, M. Deck, F. Ludwig, D. Shakirov, B.E. Rapp, K. Länge, Polymer structures on surface acoustic wave biosensors, Procedia Technology 27 (2017) 35 – 36

24. Andrii Buvailo, Yangjun Xing, Jacqueline Hines, Eric Borguet, Thin polymer film based rapid surface acoustic wave humidity sensors, Sensors and Actuators B 156 (2011) 444–449

25. Sharma, S. "Tumor markers in clinical practice: General principles and guidelines." Indian journal of medical and paediatric oncology: official journal of Indian Society of Medical & Paediatric Oncology vol. 30, 1 (2009): 1-8.

26. Hua Jiang, Wenke Lu, Guoan Zhang, Study of low insertion loss and miniaturization wavelet transform and inverse transform processor using SAW devices, Ultrasonics 53 (2013) 992–997

27. Joonhyung Lee, Youn-Suk Choi, Yeolho Lee, Hun Joo Lee, Jung Nam Lee, Sang Kyu Kim, Kyung Yeon Han, Eun Chol Cho, Jae Chan Park, Soo Suk Lee, Sensitive and Simultaneous Detection of Cardiac Markers in Human Serum Using Surface Acoustic Wave Immunosensor, Analytical Chemistry 2011, 83, 22, 8629-8635

28. Carl H. Naylor, Nicholas J. Kybert, Camilla Schneier, Jin Xi, Gabriela Romero, Jeffery G. Saven, Renyu Liu, A. T. Charlie Johnson, Scalable Production of Molybdenum Disulfide Based Biosensors, ACS Nano20161066173-6179

29. Deblina Sarkar, Wei Liu, Xuejun Xie, Aaron C. Anselmo, Samir Mitragotri, Kaustav Banerjee, MoS2 Field-Effect Transistor for Next-Generation Label-Free Biosensors, ACS Nano2014843992-4003

30. Bong Gill Choi, HoSeok Park, Tae Jung Park, Min Ho Yang, Joon Sung Kim, Sung-Yeon Jang, Nam Su Heo, Solution Chemistry of Self-Assembled Graphene Nanohybrids for High-Performance Flexible Biosensors, ACS Nano2010452910-2918

31. Shuangming Li, Ying Wan, Yan Su, Chunhai Fan, Venkat R. Bhethanabotla, Gold nanoparticle-based low limit of detection Love wave biosensorfor carcinoembryonic antigens, Biosensors and Bioelectronics 95 (2017) 48–54
32. W.J. Weber, Physicochemical Processes for Water Quality Control, Wiley-Interscience, 1972.
33. Farabi Temel, Egemen Ozcelik, Ayse Gul Ture, Mustafa Tabakci, Sensing abilities of functionalized calix[4]arene coated QCM sensors towards volatile organic compounds in aqueous media, Applied Surface Science 412 (2017) 238–251
34. M. Yang, M. Thompson, W. C. Duncan-Hewitt, Interfacial Properties and the Response of the Thickness-Shear-Mode Acoustic Wave Sensor in Liquids, Langmuir. 9 (1993) 802-811.
35. X. Zhang, Y. Zou, C. An, K. Ying, X. Chen, P. Wang, Sensitive detection of carcinoembryonic antigen in exhaled breath condensate using surface acoustic wave immunosensor, Sensors & Actuators B: Chemical, 217, 2015, 100-106.
36. Shao Su, Xiaoyan Han, Zaiwei Lu, Wei Liu, Dan Zhu, Jie Chao, Chunhai Fan, Lihua Wang,Shiping Song, Lixing Weng, and Lianhui Wang, Facile Synthesis of a MoS2−Prussian Blue Nanocube Nanohybrid-Based Electrochemical Sensing Platform for Hydrogen Peroxide and Carcinoembryonic Antigen Detection, ACS Appl. Mater. Interfaces 2017, 9, 12773−12781
37. Oh Seok Kwon, Hyun Seok Song, Tai Hyun Park, Jyongsik Jang, Conducting Nanomaterial Sensor Using Natural Receptors, Chemical Reviews 2019, 119, 1, 36-93
38. Mandana Veiseh, M. Hadi Zareie, Miqin Zhang, Highly selective Protein Patterning on Gold-Silicon Substrates for Biosensor Applications, Langmuir, 2002, 18, 17, 6671-6678.

39. Jennifer L. Trevor, Donald E. Mencer, Keith R. Lykke, Michael J. Pellin, Luke Hanley, Surface Mass Spectrometry of Biotinylated Self-Assembled Monolayers, Analytical Chemistry 1997, 69, 21, 4331-4338

Highlights

- ✓ A novel nanomaterial cluster of AuNP-MoS_2-rGO was synthesised
- ✓ Transducing bioreceptor base of PI/ AuNP-MoS_2-rGO was synthesised
- ✓ A thin film of the same was used for biosensing of CEA successfully
- ✓ Limit of detection was obtained at 0.084 ng/ml.
- ✓ The biosensor has recorded excellent stability for 70-80 days
- ✓ The biosensor was validated through clinical serum sample analysis
- ✓ The results were in line with the ELISA results of same samples.
- ✓ The biosensor has excellent selectivity towards CEA
- ✓ The study is validated with Langmuir and Freundlich adsorption isotherms.

SZU/CEP/Publication/2019-20 **25 October 2019**

The Editor
Material Chemistry and Physics

Sub: Submission of article "**Highly stable, love-mode surface acoustic wave biosensor using Au nanoparticle-MoS_2-rGO nano-cluster doped polyimide nanocomposite for the selective detection of carcinoembryonic antigen**".

Dear Sir,

I hereby agree to comply with the publishing ethics as described by journal and shall abide by the rules and regulations. The proposal has been accepted by all the authors for publishing and it is not under consideration for publication anywhere in the same form in English or in any other languages. Also, hereby declares that we do not have any sort of conflict of interest about this research article to Material Chemistry and Physics.

Kindly acknowledge & confirm the receipt of the same.
With best regards

Dr Ponnath Janardhanan Jandas
Shenzhen Key Laboratory of Advanced Thin Films and Applications,
College of Physics and Energy,
Shenzhen University,
Pin: 518060, Shenzhen, PR China
Ph: +86 13068785990